Multifunctional Coreless Hall-Effect Current Transformer for the Protection and Measurement of Power Systems

Yuan-Pin Tsai, Kun-Long Chen, Yan-Ru Chen, and Nanming Chen

***Abstract*— This paper presents a multifunctional coreless current transformer based on the Hall effect (multifunctional HCT), and designs its actual electronic circuit that can discriminate load and fault currents to perform both metering and protective functions. The multifunctional HCT has two primary circuits: 1) distinguishes the load current from the fault current and 2) delivers the current value using an analog multiplexer. This HCT can eliminate the 2.5 ± 0.05 V offset voltage of commercial Hall sensors. It possesses two amplifiers with different gains. Therefore, this multifunctional HCT accurately measures power currents during the operations in measurement systems and protection systems. Using a low-pass filter, the multifunctional HCT is not only capable of reducing noise interference, but also improves the accuracy of power current measurements. The experimental results show that the multifunctional HCT can exhibit an accuracy class of 0.5 for both the measurement and protection of power systems within IEC standard 60044-8. Because the proposed multifunctional HCT does not have core and saturation problems, the accuracy class and limit can achieve the standard accuracy limit factor grade of 63.**

***Index Terms*— Analog multiplexer, comparison circuits, current transformers, Hall-effect devices.**

I. Introduction

TRADITIONAL power systems use two modes of current transformers (CTs) and relays to monitor power feeders. However, CTs may cause distorted waves when subjected to large instantaneous fault currents. These distorted waves are closely related to the fault current offset, magnitude of the fault current, remnant magnetic flux density in the CT core, secondary circuit impedance, saturation voltage, and the turns ratio [1].

To address this problem, researchers have attempted to solve the saturation problem of the iron core. Molcrette and an IEEE work group both showed that using a small quantity of the magnetic flux in the air gap of an iron core can prevent magnetic saturation. The decay rate is, however, slower than that of a traditional CT, and thus, may cause greater error [2], [3]. Vakilian and Degeneff [4] argued that using nonmagnetic materials and a linear coupler to substitute for the iron core of a CT would eliminate magnetic saturation. In [5] and [6], the use of a magneto-optical CT composed of polished fine optical glass (i.e., a Faraday sensor or rotator) is proposed. In 1912, Rogowski and Steinhaus wound a wire compactly around a strawboard band, using the device to measure the magnetomotive force (mmf) between the two points. Rogowski coils are currently chiefly used for current measurements (e.g., the mmf of a closed path) [7]–[9]. However, the cost of Rogowski coil is high and applications are limited.

TABLE I
PERFORMANCE COMPARISON OF CURRENT SENSORS

Sensors	CTs	Rogowski Coil	Faraday sensor	Hall Sensor
Volume	Large	Small	Small	Small
Frequency Range	AC <100Hz	AC <100Hz	DC~300MHz	DC~150kHz
Sensitivity	Low	Low	High	1.3~2.5mV/G
Temperature Coefficient	--	--	−0.4 %/°C	−0.3 %/°C
Dynamic Range	--	--	0 A~3 kA	10mA~35k A

Silicon Hall sensors are widely used. In industry, they are found in contactless switches, position indicators and meters, and systems for the measurement of speed and rotation. In a power system, Hall sensors are located in systems such as current sensing and control systems. Numerous Hall probes are used in home appliances, domestic electronics, and computers.

A Hall device [10] typically has the form of a plate fitted with four contacts, similar to that with which Hall discovered his effect. The Hall device is sensitive to the magnetic field that is perpendicular to the chip plane. For applications where sensitivity to the magnetic field parallel to the device surface is preferred, a vertical Hall device has been devised [11].

Table I shows that compared with traditional CTs, the Rogowski coil, and Faraday sensor, Hall sensors have simpler structures, easier fabrication processes, and lower costs.

According to IEEE C57.13 and IEC 185 standards, the use of adequate CT accuracy class designations ensures satisfactory measurement and protection performance. Two CT modes are installed in switchgears for measuring loads and fault currents. This paper presents the development of a multifunctional HCT combining both the measurement and protection functions, and designs the actual electronic circuit to

Manuscript received January 12, 2013; revised May 21, 2013; accepted July 1, 2013. Date of publication September 24, 2013; date of current version February 5, 2014. This work was supported by the National Science Council, Republic of China under Contract NSC 97-2221-E-011-151-MY3. The Associate Editor coordinating the review process was Dr. Edoardo Fiorucci.

The authors are with the Department of Electrical Engineering, National Taiwan University of Science and Technology, Taipei 106, Taiwan (e-mail: pinnytsai@seed.net.tw; D9507103@mail.ntust.edu.tw; m10007113@mail.ntust.edu.tw; nmchen@mail.ntust.edu.tw).

Color versions of one or more of the figures in this paper are available online at http://ieeexplore.ieee.org.

Digital Object Identifier 10.1109/TIM.2013.2281555

implement this multifunctional HCT. The multifunctional HCT transforms power currents into Hall voltages and measures currents in a wide current range. Multifunctional HCTs not only filter, but also amplify Hall voltage to increase the signal-to-noise (S/N) ratio when measuring load currents. However, they scale down the Hall voltage to remain within a measurable range when measuring fault currents. This paper used low-pass filter and weighted adder circuits to regulate amplitude gains from 0 to 600 A for load currents and 600–40 kA for fault currents in two sections. Therefore, the proposed multifunctional HCT achieves both measuring and protection functions. Furthermore, the small volume of this multifunctional HCT greatly reduces the space of a switchgear.

Power currents are transformed into Hall voltages using Hall sensors in the proposed multifunctional HCT. Two circuits are used to differentiate the Hall voltage range. One circuit distinguishes the load currents from fault currents. The other, an analog multiplexer, transforms current values into accurate ratio values for loads or fault signals, whereas the multiplexer receives the compared signal from the comparison circuit. Next, a monitoring system shows the values in real load or fault current values.

Laboratory Virtual Instrument Engineering Workbench (LabVIEW) software was used to construct the measurement system in this paper. The measurement system yielded noise levels, current errors, and phase errors at different current values. According to IEC Standard 60044-8 [12], this paper shows that the proposed multifunctional HCT can achieve a class 0.5 accuracy grade in current and phase error specifications.

II. Description of the Multifunctional HCT Application Fields

Traditional CTs frequently deliver distorted waves when used to measure large instantaneous fault currents. In addition, CTs have noise interference problems when measuring low load currents. These problems may affect the safety and stability of the power systems.

The Hall sensor can measure dc and ac currents, even with complex waveforms with good accuracy, a fast time response, and wide frequency bandwidth. These characteristics make Hall sensors well suited for power system applications. The closed-loop Hall-effect current transducer is excellent for medium performance and economical applications [13]–[17].

The HCT was proposed in [18]–[20] for the measurement of power currents. In this method, four Hall sensors, used without iron cores, are symmetrically attached to a cable. This paper used a commercial Hall sensor A1302, which is a continuous-time, ratiometric, linear Hall-effect sensor. It can accurately provide a voltage output proportional to an applied magnetic field. Its linearity measure range options were 2000 G, higher than the 1000 G of A1301 [21], as shown in Table II. The simulation and measurement results show that the HCT, which averages Hall voltages use the four Hall sensors, can eliminate the ambient interference of the magnetic field in a three-phase power system.

In this method, two questions, however, have not been addressed: voltage saturation in the circuit of the amplifier and a low S/N ratio for measuring low load currents. Thus, the measuring range of the former method cannot cover both the load and fault currents. To resolve these issues, the multifunctional HCT must deliver accurate current waveforms for various loads and fault current ranges with a two-stage amplifying gain structure. In the previous paper, the current measuring range of coreless HCT for the actual power measuring condition is from a 600-A load current to an 8-kA fault current with a Class 1.0 accuracy in [19]. The other experiment for the actual power condition ranged is from a 300-A load current to a 2-kA fault current with a Class 0.5 accuracy in [20]. This paper performed comprehensive currents from 15-A load currents to 40-kA fault currents and restored the current waveforms for measurement and the protection of monitoring systems.

TABLE II
Continuous-Time, Ratio Metric Linear Hall Effect Sensors

Characteristic	A1301	A1302
Supply Voltage (VCC)	5V	5V
Output Bandwidth	20kHz	20kHz
Wide Band Output Noise, rms	150μ V	150μ V
Sensitivity (Typical)	2.5 mV/G	1.3 mV/G
Magnetic Sensitivity Error with respect to ΔV_{CC2}	±3.0%	±3.0%
Linearity	±2.5%	±2.5%
Output Voltage, Vout(High)	4.7V	4.7V
Output Voltage, Vout(Low)	0.2V	0.2V
Quiescent Output Voltage, V_{out}	±5V	±5V
Linearity Measure Range	1000G	2000G

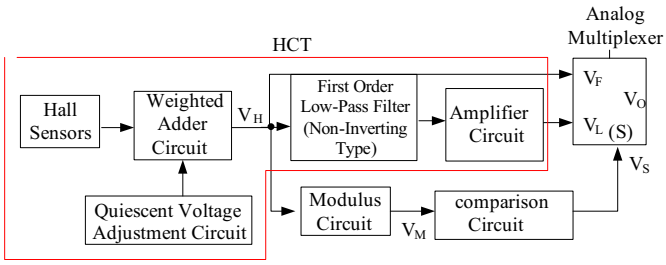

Fig. 1. Block diagram of the multifunctional HCT.

III. Innovative Structure of Multifunctional HCT

A multifunctional HCT has the following four circuits: 1) a coreless HCT; 2) a modulus circuit; 3) a comparison circuit; and 4) an analog multiplexer (Fig. 1). The HCT converts the magnetic fields generated by cable currents into Hall voltages V_H. Thereafter, quiescent voltage adjustment and weighted adder circuits reduce the gain to avoid a dc voltage offset and wave distortion for the voltage V_H. In the event of a power system failure, the voltage V_H responds to the fault currents, and V_H is directly transmitted to the input terminal V_F of an analog multiplexer. Conversely, the first-order low-pass filter with a noninverting type and an amplifier circuit increase the V_H signal value and S/N ratio when V_H responds to the load currents. The amplifier output is then sent to the terminal V_L of the analog multiplexer. V_H is modulated by

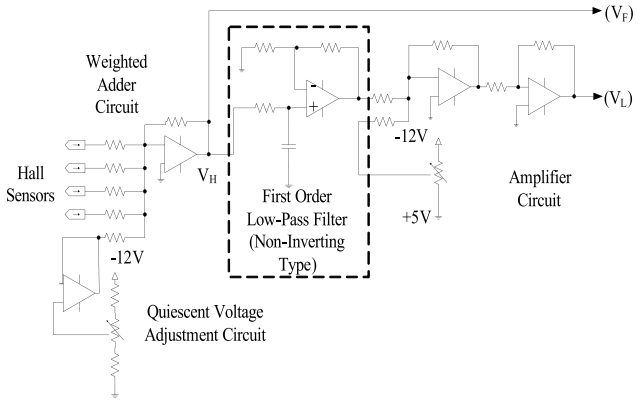

Fig. 2. HCT structure.

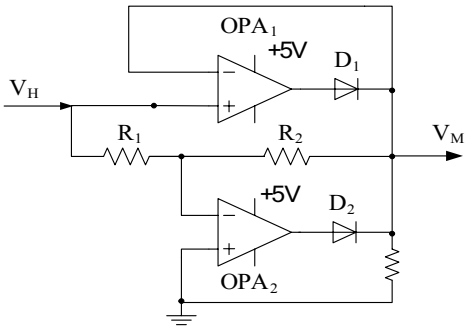

Fig. 3. Structure of the modulus circuit.

the modulus circuit as the signal V_M. The comparison circuit then distinguishes the V_M mode as a load or fault value. The signal V_S is then transmitted to the selected terminal of the analog multiplexer. Finally, the output signal V_O of the analog multiplexer shows the current mode for V_F or V_L while receiving the comparison signal V_S.

A. Structure of HCT

The application of an HCT has been addressed in [18]–[20]. A side-by-side comparison of the conventional CTs and HCTs is provided in [18]–[20]. This paper reduced the gain of the weighted adder circuit in the HCT. This function can indicate the Hall voltage V_F as a fault current. In contrast, for displaying the load current, a first-order low-pass filter with a noninverting type circuit is used to modify the HCT filter circuit to filter noise in V_H. The corner frequency of the filter is 14.468 Hz. An amplifier circuit is then used to obtain an accurate V_L, as shown in Fig. 2.

B. Modulus Circuit

During a power system failure, the signal V_H has no steady polarity value. Therefore, the comparison circuit cannot respond correctly with the V_H signal. For indicating the correct V_H signal as load or fault signatures, the multifunctional HCT uses the modulus of V_H, as shown in Fig. 3. The OPA_1 activated while the value V_H is plus, and then the OPA2 activated while the value V_H is negative. Therefore, the output

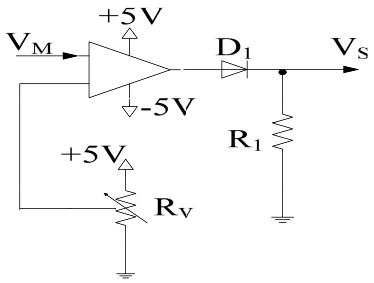

Fig. 4. Structure of the comparison circuit.

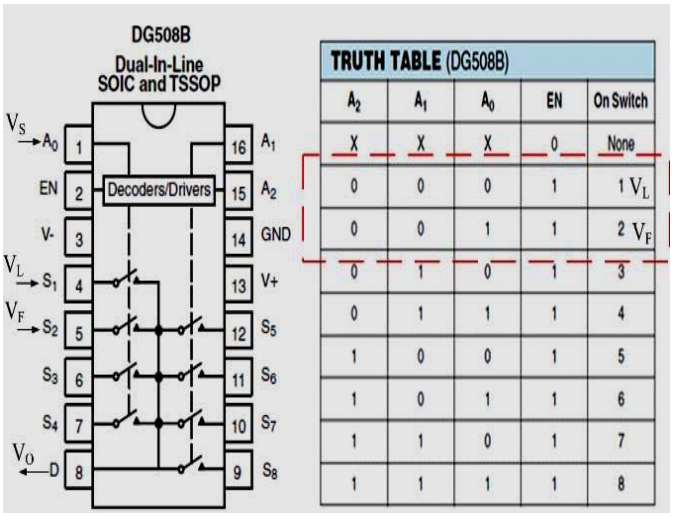

Fig. 5. Function of the analog multiplexer and truth table.

V_M always indicates a plus value V_H for current signatures. Resistances R_1 and R_2 are the same value 10 kΩ.

C. Comparison Circuit

The comparison circuit is shown in Fig. 4. The reference voltage was adjusted from 0 to 5 V by an R_V adjustable resistor. To compare V_M values with the reference voltage, the comparison circuit outputs a compared signal V_S of 5 V for a fault condition when V_M is higher than the reference voltage. Conversely, the differentiation circuit outputs a compared signal V_S of 0 V for a load condition when V_M is less than the reference voltage. The interface point of multifunctional CT is at 600-A load current, therefore, the reference voltage was set at 1.65 V by an R_V adjustable resistor for 600-A load currents.

D. Analog Multiplexer

The integrated circuit and truth table of the DG508B analog multiplexer are shown in Fig. 5 [22]. The signals connected to the terminals of DG508B include: 1) the load signal V_L that connects to S_1; 2) the fault signal V_F that connects to S_2; 3) the comparison signal V_S that connects to A_0; and 4) the output signal V_O connects to D. Terminals A_1 and A_2 are tied to ground.

Thus, their values are zero in the DG508B truth table. When V_S is 0 V, the S_1 switch turns on and transmits the signal V_L

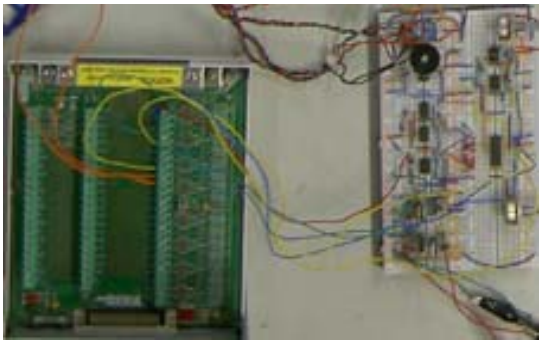

Fig. 6. Multifunctional HCT circuit and connection box.

to the terminal V_O. When V_S is 5 V, the S_2 switch turns on and transmits the signal V_F to the terminal V_O. Subsequently, the monitoring system displays the correct currents for the fault or load conditions using the analog multiplexer.

The completed multifunctional HCT circuit and connection box are as shown in Fig. 6.

IV. Framework of the Measurement System

LabVIEW is routinely used as a machine interface for measuring electric currents [23]. The monitor system compares the electric current and phase errors between the proposed multifunctional HCT and a traditional CT. Fig. 7 shows a photograph of the measurement system. The autotransformer TR1 controls transformer TR2. TR2 only has one turn in its secondary winding, which produces a large electric current under short-circuit conditions. LabVIEW was used to compare a series of waveforms generated by the multifunctional HCT with those generated by the traditional CT. The power cable that was used as a secondary winding in TR2 was a 200-mm^2 XLPE cable with a diameter of 38 mm.

When a fault occurs in a power system, the weighted adder circuit of the multifunctional HCT must reduce the amplifier gain when the Hall sensors inspect fault currents. Thus, the circuit avoids transforming wave distortion from saturation situations. In contrast, the multifunctional HCT must increase the gain when Hall sensors inspect low load currents using low-pass filter and amplifier circuits. Therefore, this circuit can accurately transform a wave to avoid noise interference. The stage amplifying gain structure has two gains for 600-A load currents and 40-kA fault currents. An amplifier gain of 66.67 is used for 0 to 600-A load currents, and an amplifier gain of one is used for 600 A to 40-kA fault currents, and 40-kA fault currents are divided by 600-A load currents to determine the amplifier gain of 66.67.

Furthermore, the weighted adder fault signal V_F and amplifier signal V_L are delivered to an analog multiplexer. The analog multiplexer differentiates measured signals between the load current V_L and fault current V_F in a switching time while the multiplexer receives an output signal V_S from the comparison circuit. The analog multiplexer outputs an accurate ratio value V_O for load or fault currents under the monitoring scale of LabVIEW system. The multifunctional HCT transforms currents into Hall voltages in a ± 5 V range.

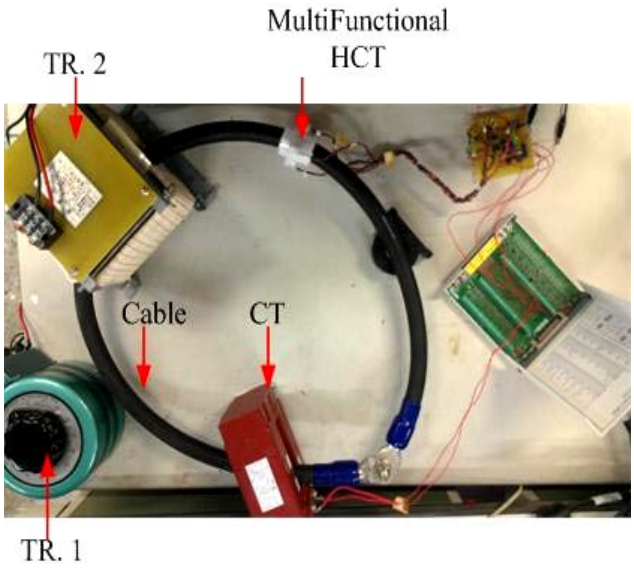

Fig. 7. Measurement system framework.

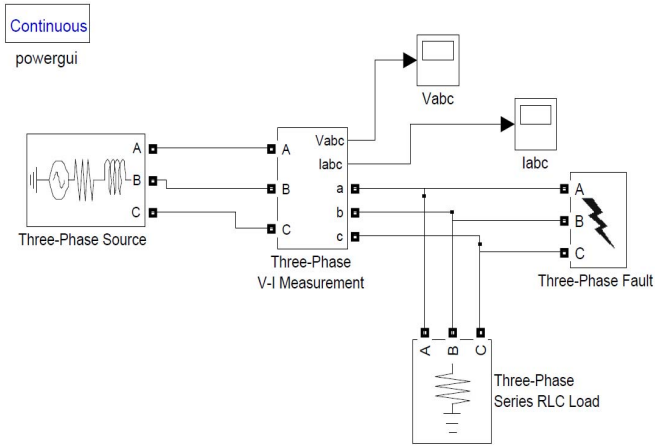

Fig. 8. 40-kA simulated fault currents by MATLAB/SIMULINK program.

Thus, the actual current level is restored for load or fault currents by LabVIEW system with class 0.5 accuracy when the LabVIEW system receives a differential signal V_S. The data acquisition board specification of the LabVIEW system is 16-b resolution, ±10 V amplitude range, and 6-kHz sampling frequency.

The 40-kA fault currents were simulated by MATLAB/SIMULINK program, as shown in Fig. 8, and then the simulated waveform was delivered into a N1-Px1 industrial computer. The fault current waveform was transformed into a proportional Hall voltage V_H, afterward the proportional Hall voltage V_H was transited to the point V_H of the multifunctional HCT, as shown in Fig. 9. The N1-Px1 industrial computer compared the output voltage V_O of the multifunctional HCT with the geometric ratio Hall voltage V_H and the computer analyzed the accuracy of the multifunctional HCT.

A. Measurement Range of Power Currents

This paper used a distribution substation (D/S) as an example. The CT ratio of the power feeder had a 600/5 multiratio

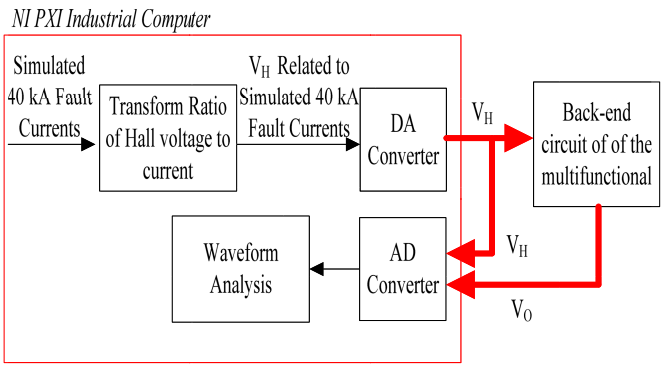

Fig. 9. 40-kA simulated fault currents measurement system framework.

TABLE III
VALUES OF FAULT CURRENTS UNDER VARIOUS FAULT CONDITIONS

Fault Type	Three-phase Fault (kA)	Line-to-Ground Fault (kA)	Line-to-Line Fault (kA)	Line-to-Line-to-Ground Fault (kA)
161 kV BUS	40.952	38.524	35.466	39.856
23.9 kV BUS	4.22	4.198	3.636	4.209
11.95 kV BUS	8.439	8.396	7.271	8.419

with a C100 rating. The maximum load current was 600 A. Various fault conditions of the D/S were simulated using a commercial software program. Table III shows the fault currents during a three-phase fault, a line-to-ground fault, a line-to-line fault, and a line-to-line-to-ground fault. The multifunctional HCT measured currents from 0 to 600 A for load currents and from 600 A to 40 kA for the fault currents in the two sections, and the LabVIEW system restores the rms waveform.

B. Limitation Values of the Multifunctional HCT

The power cable sizes were 800 mm^2 for 161 kV and 250 mm^2 for 23.9 and 11.4 kV. The radii, including the conductor and insulator, were 53.5 mm for 161 kV, 23.5 mm for 23.9 kV, and 20.5 mm for 11.4 kV, furthermore, the multifunctional HCT is fixed on the cable with a 5-mm thick insulator, as shown in Fig. 7. The relative permeability of the insulator was $\mu_r = 1$. Table IV shows the flux densities produced by (1) with the power system faults in Table III [24]. The proposed multifunctional HCT must be placed on a cable surface for detecting a high magnetic flux density because of fault currents

$$\mathbf{B} = \mathbf{a}_\phi \frac{\mu_0 I}{2\pi r} \tag{1}$$

where r is the distance from the multifunctional HCT to the center of the power cable, I is the load current or fault current flowing in the cable (rms) and μ_0 is the permeability of free space.

A commercial Hall sensor A1302 was used in the multifunctional HCT for inspecting the magnetic signatures of the currents. The peak measured magnetic flux density 0.198 T was $\sqrt{2}$ times of 0.14 T, <0.2 T of the Hall sensor A1302.

TABLE IV
MEASURED FLUX DENSITY OF MULTIFUNCTIONAL HCT BY (1) WITH THE FAULT CURRENTS SHOWN IN TABLE III

Fault Type	Three-phase Fault	Line-to-Ground Fault	Line-to-Line Fault	Line-to-Line-to-Ground Fault
	Magnetic Flux Density $\mathbf{B}$ (T)	Magnetic Flux Density $\mathbf{B}$ (T)	Magnetic Flux Density $\mathbf{B}$ (T)	Magnetic Flux Density $\mathbf{B}$ (T)
161 kV BUS	0.14	0.132	0.121	0.136
23.9 kV BUS	0.03	0.0295	0.0255	0.0295
11.95 kV BUS	0.0662	0.0659	0.057	0.066

TABLE V
SENSITIVITY OF MULTIFUNCTIONAL HCT

	Sensitivity of Hall Senaor (A1302)	Output Voltage of Hall Sensor	Amplifier Gain of Weighted Adder Circuit	The Hall Voltage V_H	Sensitivity of HCT
600A	1.3 mV/G	0.029V	66.67	1.94V	3.23 mV/A
40kA	1.3 mV/G	1.82V	1	1.82V	45.5 V/A

The sensitivity and amplifier gain of multifunctional HCT are shown in Table V.

V. EXPERIMENTAL RESULTS AND DISCUSSION

The proposed multifunctional HCT was tested through a series of current measurements, including load and fault currents, according to an accuracy class 0.5 for measuring CTs and accuracy class 5Px for protective CTs, as given in IEC Standard 60044-8. The 600A rated current of a traditional CT used in medium-voltage systems was selected as the design objective. These current tests included the measurements of: 1) the accuracy of a multifunctional HCT for 600 A rated current measurements; 2) measured current waveforms during amplification circuit switching; 3) various current levels; and 4) simulated 40kA fault currents.

A. Accuracy of the Multifunctional HCT for 600 A Rated Current Measurement

With IEC Standard 60044-8, the proposed multifunctional HCT should be tested under 5%, 20%, 100%, and 120% of the rated currents. The test results current errors, and phase errors were measured to check the accuracy class. This paper addressed both the 600-A rated current and the 0.5 accuracy class for the design of a multifunctional HCT. Tables VI and VII show the measurement results. The reference currents were based on traditional CTs with an accuracy class of 0.2. All the current and phase errors were smaller than the standard limits. Thus, the proposed multifunctional HCT achieves an accuracy class of 0.5 within IEC Standard 60044-8.

B. Measured Current Waveforms During Amplification Circuit Switching

The current waveforms were measured under the following different conditions: 1) before the amplification circuit

TABLE VI
CURRENT ERRORS OF THE MULTIFUNCTIONAL HCT AT A 600-A RATED CURRENT

Item	Percentage Current Error (%) at Percentage of Rate Current Shown Below.			
	5	20	100	120
Accuracy Class 0.5 of IEC Standard 60044-8	1.5	0.75	0.5	0.5
Measurement Results of Multifunctional HCT	0.368	0.396	0.028	0.465

TABLE VII
PHASE ERRORS OF THE MULTIFUNCTIONAL HCT AT A 600-A RATED CURRENT

Item	Phase Error (deg.) at Percentage of Rate Current Shown Below.			
	5	20	100	120
Accuracy Class 0.5 of IEC Standard 60044-8	2.7	1.35	0.9	0.9
Measurement Results of Multifunctional HCT	0.106	0.163	0.085	0.093

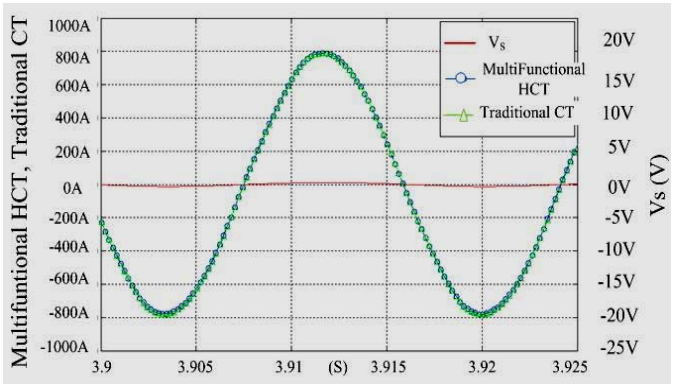

Fig. 10. Comparison between the current waveforms measured by the multifunctional HCT and traditional CTs at a 550-A rated current.

switched when the load current was ∼550 A; 2) under threshold load currents during the amplification circuit switching with a load current of ∼600 A; and 3) the current waveforms switched with load currents of ∼650 A. Figs. 10–12 show the comparisons of the current waveforms measured by the multifunctional HCT and traditional CTs at rated currents of 550, 600, and 650 A, with the corresponding errors shown in Tables VIII–X, respectively. In Fig. 10, the current waveform of the multifunctional HCT exhibited the same waveform for CTs because the load current of 550 A was smaller than the threshold current. Conversely, the current waveform of the multifunctional HCT was outputted from the two stages of amplifiers in Fig. 11 because the load current of 600 A was larger than the threshold current. The current waveform combination was similar to a sine wave. Furthermore, the switching impulse in the current waveform measured by the multifunctional HCT results from a time delay in the

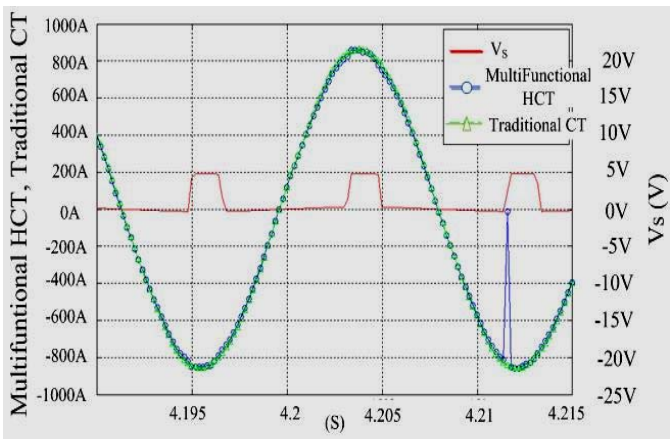

Fig. 11. Comparison between the current waveforms measured by the multifunctional HCT and traditional CTs at a 600-A rated current.

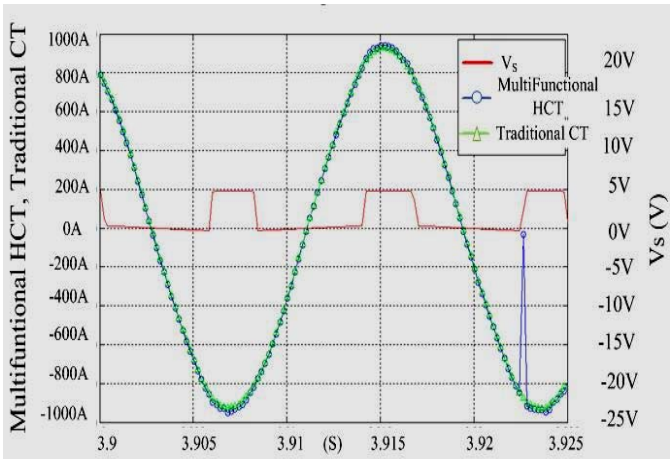

Fig. 12. Comparison between the current waveforms measured by the multifunctional HCT and traditional CTs at a 650-A rated current.

transmission of the analog multiplexer. When the V_S signal is simultaneously transmitted to the analog multiplexer and the measurement systems, the analog multiplexer detects the rising voltage edge, up to 2 V, and then outputs the corresponding signal. The switching time is ∼0.4 ms. The area ratio of the switching impulse to the whole waveform does not increase as the load current increases, as shown in Fig. 12. The multifunctional HCT achieves an accuracy class of 0.5 within IEC Standard 60044-8.

C. Measurements of Different Current Levels

Waveforms are measured at various current levels as shown in Table XI, when the current level was increased by 100 A from a level of 100 A. When the load current was 600 A, the percentage current and phase errors achieved a minimum. In addition, the percentage current and phase errors increased when the current level decreased. The percentage current error was however, <0.4% when the current level was 100 A. Furthermore, the percentage current and phase errors increased when the current level increased. The percentage current error was, however, still <0.2%. All the phase errors were <1° and independent of current levels. The percentage current errors

TABLE VIII
CURRENT AND PHASE ERRORS BETWEEN CURRENT WAVEFORMS MEASURED BY THE MULTIFUNCTIONAL HCT AND TRADITIONAL CTS AT A 550-A RATED CURRENT

	Item	Value
1	Hall Current (DC)	9.14256A
2	Hall Current (Peak to Peak)	1577.3A
3	Hall Current (RMS)	552.223A
4	Traditional Current (DC)	1.63531A
5	Traditional Current (Peak to Peak)	1579.77A
6	Traditional Current (RMS)	552.153A
7	Current Phase Delay	0.113283°
8	Percentage Current Error	-0.168402%

TABLE IX
CURRENT AND PHASE ERRORS BETWEEN CURRENT WAVEFORMS MEASURED BY THE MULTIFUNCTIONAL HCT AND TRADITIONAL CTS AT A 600-A RATED CURRENT

	Item	Value
1	Hall Current (DC)	-1.57557A
2	Hall Current (Peak to Peak)	1754.58A
3	Hall Current (RMS)	596.383A
4	Traditional Current (DC)	1.60338A
5	Traditional Current (Peak to Peak)	1706.05A
6	Traditional Current (RMS)	596.211A
7	Current Phase Delay	0.085265°
8	Percentage Current Error	0.028954%

TABLE X
PERCENTAGE CURRENT ERROR BETWEEN CURRENT WAVEFORMS MEASURED BY THE MULTIFUNCTIONAL HCT AND TRADITIONAL CTS AT A 650-A RATED CURRENT

	Item	Value
1	Hall Current (DC)	-3.82042A
2	Hall Current (Peak to Peak)	1916.73A
3	Hall Current (RMS)	655.483A
4	Traditional Current (DC)	1.25216A
5	Traditional Current (Peak to Peak)	1864.55A
6	Traditional Current (RMS)	652.387A
7	Current Phase Delay	0.043632°
8	Percentage Current Error	0.474444%

increased more quickly as the current level decreased from 100 A; however, the percentage current error is still $<1\%$ when the current level is down to 15 A.

D. Behavior Under Simulated 40-kA Fault Currents

This paper performed fault simulation using MATLAB/SIMULINK. One-quarter of the 600 A rated current (i.e., 150 A) was simulated and the magnitude of this current jumped to a 40 kA fault current when a simulated fault occurred, as shown Fig. 8. Thereafter, the simulation current waveforms were transformed into Hall voltages V_H that were outputted to the V_H connection point of the multifunctional HCT of Fig. 9. Therefore, the tests showed the response and accuracy classes of current changes when serious faults occurred. Figs. 13 and 14 show the current waveforms of the multifunctional HCT. The currents settled when a simulated fault occurred. The percentage current and phase errors are shown in Table XII. As shown by these results, the multifunctional HCT promptly responds to the waveform of a simulated fault current, including the first peak after a simulated fault occurs. The percentage current error was only 0.92%, far

TABLE XI
PERCENTAGE CURRENT AND PHASE ERRORS BETWEEN THE CURRENT WAVEFORMS MEASURED BY THE MULTIFUNCTIONAL HCT AND TRADITIONAL CTS AT DIFFERENT CURRENT LEVELS

Current Levels (A)	Percentage Current Error (%) at Different Current Levels.	Phase Error (deg.) at Different Current Levels.
15	0.907	0.311
60	0.364	0.217
100	0.302	0.171
200	0.273	0.133
300	0.312	0.127
400	0.38	0.126
500	0.425	0.136
600	0.028	0.085
700	0.081	0.51
800	0.145	0.618
900	0.147	0.622
1000	0.101	0.501

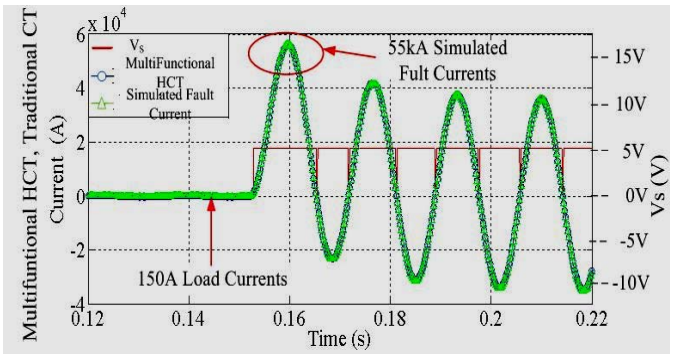

Fig. 13. Comparison between the current waveforms measured by the multifunctional HCT, the actual current waveform when a simulated fault occurred, and when the simulated fault current reached 40 kA.

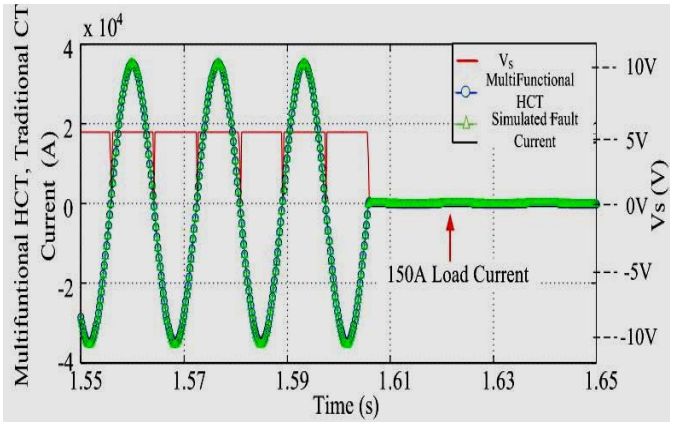

Fig. 14. Comparison between the current waveforms measured by the multifunctional HCT and simulation current waveform after the 40-kA simulated fault current settled.

TABLE XII
PERCENTAGE CURRENT AND PHASE ERROR BETWEEN THE CURRENT WAVEFORMS MEASURED BY THE MULTIFUNCTIONAL HCT AND THE SIMULATION CURRENT WAVEFORM WHEN A 40-KA SIMULATED FAULT OCCURRED

	Item	Value
1	Hall Current (DC)	-788.314A
2	Hall Current (Peak to Peak)	91271.9A
3	Hall Current (RMS)	13674.1A
4	Traditional Current (DC)	-817.622A
5	Traditional Current (Peak to Peak)	92007.9A
6	Traditional Current (RMS)	13800.5A
7	Current Phase Delay	0.016564°
8	Percentage Current Error	-0.92%

smaller than 5%. Thus, the multifunctional HCT achieved the standard accuracy limit factor grade of 63 for electronic CTs, as given by IEC Standard 60044-8.

VI. CONCLUSION

A multifunctional HCT for the protection and measurement of power systems was designed in this paper, and the electronic circuit to achieve both the functions is introduced and tested in this paper. In view of the following problems, accuracy classes for measuring a wide range of currents and circuit saturations in large current measurements, the multifunctional HCT is designed with two amplification circuits. The current measurements are divided into two separate ranges. Because each range of current measurements has its corresponding amplification circuit, measurement results become more accurate and easier to acquire and display directly. Furthermore, the proposed comparison circuit enables the measurement monitoring system to discriminate between the load and fault currents with the compared signal. Measured waveforms are restored to their actual current levels with the correct amplification ratios.

The proposed multifunctional HCT was tested under a series of current measurements according to IEC Standard 60044-8. The measurement results showed that the multifunctional HCT meet has an accuracy class of 0.5 for measuring CTs and a standard accuracy limit factor grade of 63 for protective CTs.

REFERENCES

[1] *IEEE Guide for the Applications of Current Transformers Used for Protective Relaying Purposes*, IEEE Standard C37.110-1996, 1996.

[2] An IEEE Power System Relay Relaying Committee Report, "Gapped core current transformer characteristics and performance," *IEEE Trans. Power Delivery*, vol. 5, no. 4, pp. 1732–1740, Nov. 1990.

[3] V. Molcrette, J. L. Kotony, J. P. Swan, and J. F. Brudny, "Reduction of inrush current in single-phase transformer using virtual air gap technique," *IEEE Trans. Magn.*, vol. 34, no. 4, pp. 1192–1194, Jul. 1998.

[4] M. Vakilian and R. C. Degeneff, "A method for modeling nonlinear core characteristics of transformers during transient," *IEEE Trans. Power Delivery*, vol. 9, no. 4, pp. 1916–1925, Oct. 1994.

[5] J. Song, P. G. McLaren, D. J. Thomson, and R. L. Middleton, "A clamp-on magneto-optical current transducer for power systems," in *Proc. Can. Conf. Electr. Comput. Eng.*, vol. 2. May 1996, pp. 884–887.

[6] A. Cruden, Z. J. Richardson, J. R. McDonald, I. Andonovic, W. Laycock, and A. Bennett, "Compact 132 kV combined optical voltage and current measurement system," *IEEE Trans. Instrum. Meas.*, vol. 47, no. 1, pp. 219–223, Feb. 1998.

[7] A. P. Chattock, "On a magnetic potentiometer," *Phil. Mag. J. Sci.*, vol. 24, no. 5, p. 9696, Jul./Dec. 1887.

[8] W. Rogowski and W. Steinhaus, "Die Messung der magnetischen spannung. Messung des linienintegrals der magnetischen feldstarke," *Archivfur Elektrotechnik*, vol. 1, no. 4, pp. 141–150, 1912.

[9] M. Chiampi, G. Crotti, and A. Morando, "Evaluation of flexible Rogowski coil performances in power frequency applications," *IEEE Trans. Instrum. Meas.*, vol. 60, no. 3, pp. 854–862, Mar. 2011.

[10] E. H. Hall, "On a new action of the magnet on electric currents," *Amer. J. Math.*, vol. 2, no. 3, pp. 287–292, 1879.

[11] R. S. Popovic, "The vertical Hall-effect-device," *IEEE, Electr. Devices. Lett.*, vol. 5, no. 9, pp. 357–358, Sep. 1984.

[12] *Instrument Transformers-Part 8: Electronic Current Transformers*, IEC Standard 60044-8, Jul. 2002.

[13] M. Etter and M. Friot, "Wide bandwidth, accurate current, and voltage transducers," in *Proc. PCIM Eur.*, Nov./Dec. 1993, pp. 1–32.

[14] H. C. Appello, M. Groenenboom, and J. Lisser, "The zero-flux DC current transformer: A high precision bipolar wide-band measuring device," *IEEE Trans. Nuclear Sci.*, vol. 24, no. 3, pp. 1810–1811, Jun. 1977.

[15] X. Ai, H. Bao, and Y. H. Song, "Novel method of error current compensation for Hall-effect-based high-accuracy current transformer," *IEEE Trans. Power Delivery*, vol. 20, no. 1, pp. 11–14, Jan. 2005.

[16] C. Schott, F. Burger, H. Blanchard, and L. Chiesi, "Modern integrated silicon Hall sensors," *Sensor Rev.*, vol. 18 , no. 4, pp. 252–257, 1998.

[17] L. Cristaldi, A. Ferrero, M. Lazzaroni, and R. Ottoboni, "A linearization method for commercial Hall-effect current transducers," *IEEE Trans. Instrum. Meas.*, vol. 50, no. 5, pp. 1149–1153, Oct. 2001.

[18] N. Chen and Y. P. Tsai, "Power current micro sensor," U.S. Patent I263 050, Oct. 1, 2006.

[19] K. L. Chen and N. Chen, "A new method for power current measurement using a coreless Hall effect current transformer," *IEEE Trans. Instrum. Meas.*, vol. 60, no. 1, pp. 158–169, Jan. 2011.

[20] K. L. Chen, Y. P. Tsai, N. Chen, S. K. Korkua, and W.-J. Lee, "Using coreless Hall effect sensor for accurate current measurement in ZigBee based wireless sensor network," in *Proc. IAS Annu. Meeting*, Oct. 2011, pp. 1–8.

[21] *A1301 and A1302 Datasheets*, Allegro MicroSstems, Inc., Worcester, MA, USA, 2005.

[22] *Precision 8-Channel / Dual 4-Channel CMOS Analog Multiplexers Datasheet*, VishayIntertechnology, Inc., Malvern, PA, USA, Dec. 2010.

[23] *LabVIEW User Manual*, Nat. Instrum. Corp., Maryland, MD, USA, 2000.

[24] D. K. Cheng, *Field and Wave Electromagnetics*. Toronto, ON, Canada: Addison-Wesley, 1989, pp. 321–345.

Yuan-Pin Tsai was born in Chiayi, Taiwan, in 1965. He received the B.S.E.E. and M.S.E.E. degrees from the National Taiwan University of Science and Technology, Taipei, Taiwan, in 1992 and 2004, respectively, where he is currently pursuing the Ph.D. degree with the Department of Electrical Engineering.

He has been with Taiwan Electrical and Mechanical Engineering Services, Inc., Taipei, since 1992, where he is a Project Manager. His current research interests include power system protection and electrical safety.

Kun-Long Chen was born in Taipei, Taiwan, in 1982. He received the B.S.E.E. degree from Feng-Chia University, Taichung, Taiwan, in 2004, and the M.S.E.E. and Ph.D. degrees from the National Taiwan University of Science and Technology, Taipei, in 2006 and 2011, respectively.

He has been a Researcher with Industrial Technology Research Institute, Hsinchu, Taiwan, since 2011. His current research interests include current sensors and electrical energy metrology for smart grid.

Yan-Ru Chen was born in Taipei, Taiwan, in 1989. He received the B.S.E.E. degree from the National Taiwan University of Science and Technology, Taipei, in 2011, where he is currently pursuing the master's degree with the Department of Electrical Engineering.

His current research interests include current sensors and their applications in power systems.

Nanming Chen was born in Taiwan in 1951. He received the B.S.E.E. degree from National Taiwan University, Taipei, Taiwan, in 1973, the M.S.E.E. degree from Virginia Polytechnic Institute and State University, Blacksburg, VA, USA, in 1977, and the Ph.D. degree from Purdue University, West Lafayette, IN, USA, in 1980.

He was with Pacific Gas and Electric Company and San Francisco State University, San Francisco, CA, USA. Since 1989, he has been a Professor with the Department of Electrical Engineering, National Taiwan University of Science and Technology, Taipei. His current research interests include power engineering and electrical railway system.

Dr. Chen was the Director on the board of directors of Taiwan Power Company from 2004 to 2007 and Stability and Reliability Committee of TPC from 2001 to 2003. He was appointed as a member of the Blackout Investigation Committee in 1999 and 3rd Nuclear Power Plant Blackout Investigation Committee in 2001.